Nonlinear and diffraction effects in propagation of *N*-waves in randomly inhomogeneous moving media

Mikhail Averiyanov[a)]
Faculty of Physics, Moscow State University, Moscow, Russia

Philippe Blanc-Benon
LMFA UMR CNRS 5509, Ecole Centrale de Lyon, 69134 Ecully Cedex, France

Robin O. Cleveland
Department of Mechanical Engineering, Boston University, Boston, Massachusetts 02215

Vera Khokhlova[b)]
Faculty of Physics, Moscow State University, Moscow, Russia

(Received 15 July 2010; revised 17 January 2011; accepted 20 January 2011)

Finite amplitude acoustic wave propagation through atmospheric turbulence is modeled using a Khokhlov–Zabolotskaya–Kuznetsov (KZK)-type equation. The equation accounts for the combined effects of nonlinearity, diffraction, absorption, and vectorial inhomogeneities of the medium. A numerical algorithm is developed which uses a shock capturing scheme to reduce the number of temporal grid points. The inhomogeneous medium is modeled using random Fourier modes technique. Propagation of *N*-waves through the medium produces regions of focusing and defocusing that is consistent with geometrical ray theory. However, differences up to ten wavelengths are observed in the locations of fist foci. Nonlinear effects are shown to enhance local focusing, increase the maximum peak pressure (up to 60%), and decrease the shock rise time (about 30 times). Although the peak pressure increases and the rise time decreases in focal regions, statistical analysis across the entire wavefront at a distance 120 wavelengths from the source indicates that turbulence: decreases the mean time-of-flight by 15% of a pulse duration, decreases the mean peak pressure by 6%, and increases the mean rise time by almost 100%. The peak pressure and the arrival time are primarily governed by large scale inhomogeneities, while the rise time is also sensitive to small scales.
 [DOI: 10.1121/1.3557034]

PACS number(s): 43.28.Mw, 43.28.Gp, 43.28.Lv [VEO] Pages: 1760–1772

I. INTRODUCTION

Both linear and finite amplitude acoustic wave propagation through turbulence are strongly affected by wind velocity fluctuations through convection of the wavefronts.[1–4] The propagation of linear acoustic signals in an inhomogeneous moving medium has been widely investigated, for example, within the high frequency approximation[5–7] and using the wide angle parabolic approximation.[8–10] Linear scattering of sound waves on random scalar inhomogeneities have also been considered using Born approximation.[11] Focusing of high amplitude and wide band acoustic signals has been considered either in homogeneous medium giving the initial distortion of the wavefront[12–14] or in media with deterministic inhomogeneity.[15,16] The diffraction of nonlinear acoustic pulses from random structures has only been reported for media with scalar type inhomogeneities.[17] To our knowledge, nonlinear focusing of wide band acoustic signals in a medium with random distribution of flow velocity has not yet been considered.

This work is partially motivated by the case of sonic boom propagation, where both numerical simulations[11,17,18] and experimental studies[19–22] have shown that the fluctuations produce random focusing and defocusing of the acoustic wave leading to significant changes in the statistics of the acoustic wave parameters, e.g., shocks with high peak pressures and short rise times can be observed in focal regions. Changes in the acoustic parameters results in corresponding changes in annoyance and subjective loudness of sonic booms.[23,24] The perceived loudness of sonic booms heard outdoors is an important factor of acceptability of supersonic flights overland.[25] Typical peak overpressure measured at the ground level in sonic boom experiments with small size aircraft are of the order of 100 Pa,[19] which corresponds to an incident pressure amplitude of 50 Pa (as the ground reflection results in a near pressure doubling at the microphone). The characteristic nonlinear distance given by this overpressure is of the order of 10 km, which is very long comparable to the width of the turbulence boundary layer (TBL). This suggests that sonic boom propagation through TBL could be considered as linear. However, atmospheric conditions or aircraft maneuvers can result in focal regions in which overpressures more than 600 Pa have been reported[19,26]; in this case nonlinear effects during propagation through the TBL may become important.

[a)]Author to whom correspondence should be addressed. Electronic mail: misha@acs366.phys.msu.ru
[b)]Center for Industrial and Medical Ultrasound, APL, University of Washington, Seattle, Washington 98105.

 0001-4966/2011/129(4)/1760/13/$30.00

The goal of this paper is therefore to study the focusing of nonlinear acoustic pulses in a moving randomly inhomogeneous medium. For this purpose, a nonlinear parabolic sound propagation model based on a Khokhlov–Zabolotskaya–Kuznetsov (KZK)-type evolution equation is used.[18] The advantage of this model is that, besides conventional nonlinear and diffraction effects, it also accounts for both longitudinal and lateral fluctuations of the turbulent velocity field. Random single and multiscale velocity fields are generated using a turbulence model based on a random Fourier Modes technique.[6] Using the model for inhomogeneities randomly distributed in space permits investigation of pressure field statistics in the presence of turbulence. Therefore, the advance reported here is to investigate the influence of nonlinear-diffraction effects on the statistics and peak values of the N-wave parameters in media with random vectorial inhomogeneities.

The paper is organized as follows: in Sec. II, the theoretical model based on the KZK-type evolution equation is described together with a model of the random velocity field. Section III contains a description of numerical algorithm used to solve the model equation.

In Sec. IV, the effects of diffraction, nonlinearity, and randomly inhomogeneous velocity fields on high amplitude N-wave focusing are presented and the statistics of a number of wave field parameters is analyzed.

II. THEORETICAL MODEL

A. Evolution equation for nonlinear waves in inhomogeneous moving medium

A nonlinear evolution equation, which accounts for fluctuations in sound speed, density, and all components of the velocity of the moving medium, has been derived within the parabolic approximation in Ref. 18. For this work, we neglect terms with scalar inhomogeneities, that is, fluctuations of medium density and speed of sound, and the resulting model equation is

$$\frac{\partial}{\partial\tau}\left[\frac{\partial p}{\partial x}-\frac{\beta}{c_0^3\rho_0}p\frac{\partial p}{\partial\tau}-\frac{\delta}{2c_0^3}\frac{\partial^2 p}{\partial\tau^2}-\frac{u_x}{c_0^2}\frac{\partial p}{\partial\tau}+\frac{1}{c_0}(\mathbf{u}_\perp\cdot\nabla_\perp p)\right]=\frac{c_0}{2}\Delta_\perp p. \quad (1)$$

Here, p is the acoustic pressure, $\tau=t-x/c_0$ is the retarded time, x is the propagation coordinate, y and z are the transverse coordinates, c_0 is the ambient sound speed, u_x is the longitudinal component of the flow in the medium, $\mathbf{u}_\perp=(u_y,u_z)$ is the transverse component of the flow, ρ_0 is the ambient density of the medium, β is the coefficient of nonlinearity, δ is the diffusivity of sound, and $\nabla_\perp=(\partial/\partial y,\partial/\partial z), \Delta_\perp=\nabla_\perp^2$.

Equation (1) is a KZK-type equation, where the first term accounts for propagation, the second term for nonlinear distortion, the third for thermoviscous absorption, the fourth for flow inhomogeneities in the propagation direction, and the fifth for transverse flow inhomogeneities. The right-hand side accounts for the effects of diffraction in the parabolic approximation. The validity of the model is restricted to smooth velocity inhomogeneities with small Mach numbers $u/c_0\ll 1$, which primarily results in scattering in the forward direction up to 20° off axis.[27]

In two-dimensional (2D) Cartesian coordinates and in dimensionless variables, Eq. (1) can be cast as

$$\frac{\partial}{\partial\theta}\left[\frac{\partial V}{\partial\sigma}-NV\frac{\partial V}{\partial\theta}-A\frac{\partial^2 V}{\partial\theta^2}-2\pi U_{||}\frac{\partial V}{\partial\theta}+U_\perp\frac{\partial V}{\partial\rho}\right]=\frac{1}{4\pi}\frac{\partial^2 V}{\partial\rho^2}. \quad (2)$$

Here $V=p/p_0$ is the acoustic pressure normalized by the pulse amplitude p_0, $\sigma=x/\lambda$ is the propagation distance and $\rho=y/\lambda$ is the transverse spatial coordinate, both normalized by the initial pulse length λ, and $\theta=2\pi\tau/T_0$ is the time normalized by the initial duration of the pulse T_0 (the initial pulse length and duration are related by $\lambda=c_0T_0$). The dimensionless nonlinearity parameter is given by $N=\lambda/x_n$, where $x_n=T_0c_0^3\rho_0/2\pi\beta p_0$ is the characteristic distance at which the amplitude of a plane N-wave decreases by a factor of $\sqrt{2}$. The dimensionless parameters $U_{||}=u_x/c_0$ and $U_\perp=u_y/c_0$ are the longitudinal and the transverse components of the velocity field, normalized by the sound speed, and $A=2\pi^2\delta/(c_0\lambda)$ is the dimensionless absorption parameter.

A typical value of the dimensionless nonlinearity parameter for sonic booms in the atmosphere is $N\simeq 0.0025$ ($p_0\simeq 50$ Pa).[19,25] As noted in the introduction, this results in almost linear acoustic wave propagation. However, peak pressures more than 600 Pa have been measured associated with focusing of sonic boom waveforms.[19,26] Therefore, in these simulations, three values of N are considered: $N=0$ which results in linear propagation, $N=0.025$ corresponding to $p_0\simeq 450$ Pa, and $N=0.05$ corresponding to $p_0\simeq 900$ Pa in order to evaluate nonlinearity beyond the range observed in sonic booms. The wind velocity in the turbulent atmosphere during sonic boom experiments was up to 15 m/s (Ref. 19), which results in the dimensionless parameters for the velocity fluctuations $U_{||,\perp}\simeq 0.04$. The dimensionless absorption parameter depends on the acoustic wavelength and for a boom generated by an aircraft of the order of 50 m one obtains the dimensionless absorption parameter $A\sim 3.6\cdot 10^{-8}$. Note that for realistic modeling of the shock front in air one needs to account for relaxation processes which affect absorption and dispersion.[28] In this paper the relaxation effects are not taken into account as the emphasis is on the effects of random inhomogeneities, nonlinearity, and diffraction rather than the details of the shock front. By modeling relaxation processes in air one predicts about a 20-fold increase in attenuation for a wavelength of 50 m, that is, the effective absorption for sonic boom frequencies is $A\sim 6\cdot 10^{-6}$. For the simulations employed here, both of these values of A were too small to ensure a stable solution with a reasonable size grid and therefore a value of $A=3.4\cdot 10^{-4}$ was used for the simulations.

B. Geometrical acoustics equations

The geometrical acoustics approach was used to trace acoustic rays and to determine the positions of caustics along ray paths in an inhomogeneous moving medium. The ray tracing equations were developed from the eikonal equation for a moving inhomogeneous medium[1,7,29] and in the absence of scalar inhomogeneities they take the form

$$\frac{dx_i}{dt} = \frac{c_0 k_i}{1 - \mathbf{l}\cdot\mathbf{u}/c_0} + u_i, \qquad \frac{dk_i}{dt} = -k_j \frac{\partial}{\partial r_i} u_j. \tag{3}$$

Here the variable t is the travel time of the acoustic pulse along a given ray, $\mathbf{r} = (x, y, z)$ is the location of the ray in space, $\mathbf{k}$ is the nondimensional wave vector, $\mathbf{l} = \mathbf{k}/|\mathbf{k}|$ is the unit vector in the direction of wave vector, and i and j indicate either the x, y, or z component of the corresponding vector.

The ray trajectory is completely determined by the distribution of medium inhomogeneities and by initial conditions given at time $t = 0$. For a plane wave and 2D Cartesian geometry, the initial conditions can be written as

$$\mathbf{r}_0 = \begin{pmatrix} 0 \\ y_0 \end{pmatrix}; \quad \mathbf{k}_0 = \frac{1}{1 + u_x/c_0}\begin{pmatrix} 1 \\ 0 \end{pmatrix}. \tag{4}$$

The location of caustics was determined by solving the system of equations for geodesic elements $\mathbf{R} = (\partial\mathbf{r}/\partial y_0)_t$, which follow the ray tube section, and by defining positions of caustics by the condition $\mathbf{R} = 0$ (Ref. 30),

$$\begin{aligned} \frac{dR_i}{dt} &= \frac{c_0}{k}\left(Q_i - \frac{k_i k_m}{k^2} Q_m\right) + R_j \frac{\partial u_i}{\partial r_j}, \\ \frac{dQ_i}{dt} &= -Q_j \frac{\partial u_j}{\partial r_i} - k_j R_m \frac{\partial^2 u_j}{\partial r_i \partial r_m}, \end{aligned} \tag{5}$$

where $\mathbf{Q} = (\partial\mathbf{k}/\partial y_0)_t$ designates "conjugate" elements. Appropriate initial conditions for the system of Eq. (5) are

$$\mathbf{R}_0 = \begin{pmatrix} 0 \\ 1 \end{pmatrix}; \quad \mathbf{Q}_0 = \frac{\partial k}{\partial y_0}\begin{pmatrix} 1 \\ 0 \end{pmatrix} = \frac{p_x^2}{c_0}\frac{\partial u_x}{\partial y_0}\begin{pmatrix} 1 \\ 0 \end{pmatrix}. \tag{6}$$

C. Inhomogeneous velocity field

A model of randomly oriented spatial Fourier modes was employed here to generate random inhomogeneous velocity fields.[6] This model is valid under the assumption that the travel time of the acoustic wave through the inhomogeneity is much smaller than the characteristic time of the evolution of the turbulence, i.e., the inhomogeneities are considered to be "frozen." The frozen inhomogeneous field was generated by summation of $J_{\max}$ random modes,

$$\mathbf{u}(\mathbf{r}) = \sum_{j=1}^{J_{\max}} \widetilde{\mathbf{U}}(\mathbf{K}_j)\cdot\cos(\mathbf{K}_j\cdot\mathbf{r} + \phi_j), \tag{7}$$

$$\widetilde{\mathbf{U}}(\mathbf{K}_j)\cdot\mathbf{K}_j = 0. \tag{8}$$

Here $\mathbf{K}_j$ is the wave vector, ϕ_j is the phase of jth Fourier mode. The angle θ_j between $\mathbf{K}_j$ and x axis, and phase ϕ_j for each mode was taken from the independent random number sequences with uniform distributions within the interval $[0, 2\pi]$. Equation (8) is the consequence of velocity field incompressibility which is justified by the small Mach numbers used in modeling. The velocity amplitude of each mode $|\widetilde{\mathbf{U}}(\mathbf{K}_j)|$ in Eq. (7) was determined by the kinetic energy spectrum $E(K)$: $|\widetilde{\mathbf{U}}(\mathbf{K}_j)|\sqrt{E(K)}, K = |\mathbf{K}|$.

Two different formulations for the turbulence energy spectrum were considered: Gaussian and modified von Kármán. Gaussian energy spectrum describes a single-scale inhomogeneous medium and in 2D geometry is

$$E(K) = \frac{1}{8}\sigma_u^2 K^3 L^4 \exp\left(-\frac{K^2 L^2}{4}\right), \tag{9}$$

where σ_u^2 is the variance of medium velocity fluctuations and L is the characteristic scale of randomly inhomogeneous medium. The modified von Kármán energy spectrum,

$$E(K) = 8\sigma_u^2 \frac{K^3}{L_0^{2/3}\left(K^2 + 1/L_0^2\right)^{14/6}} \exp\left(-\frac{K^2}{K_m^2}\right), \tag{10}$$

describes a multiscale turbulence, including the inertial interval given by Kolmogorov's "five thirds" power law, and therefore, is closer to the spectrum of real atmosphere.[31,32] Here L_0 and l_0 are the outer and inner turbulent scales, respectively, and $K_m = 5.92/l_0$ is the Kolmogorov wave number.

If a sufficiently high number of modes is included in Eq. (7) and each of the modes is randomly chosen with uniform probability distribution of θ_j and ϕ_j, then the resulting velocity field $\mathbf{u}(\mathbf{r})$ is statistically homogeneous, isotropic, and has an *a priori* defined energy spectrum.[6] In this work, random velocity fields with the Gaussian spectrum were modeled using 300 Fourier modes uniformly distributed between wave numbers $0.01/L$ and $9.0/L$. Velocity fields with the modified von Kármán spectrum were modeled using 600 Fourier modes (for better discretization of the inertial zone), logarithmically distributed between $K_{\min} = 0.01/L_0$ and $K_{\max} = 4.0/l_0$. The inhomogeneity outer scale L_0 was chosen the same as the characteristic scale L given by the Gaussian energy spectrum: $L_0 = L = 4\lambda$. The inner scale was chosen as $l_0 = 0.8\lambda$. The root mean square value of the velocity fluctuations for both spectra was $\sigma_u = 3$ m/s, which resulted in velocity fluctuations of about 15 m/s. Thus, both the outer length scale of the inhomogeneities and the amplitude of velocity fluctuations were chosen according to experimentally observed meteorological conditions.[33,34] The model of kinematic turbulence presented here does not pretend to fully reproduce the complexity of turbulent boundary layer, including its anisotropy, stratification, fluctuations in temperature, and density. However, this model is sufficiently flexible and most of the listed effects, including turbulence anisotropy, could be incorporated.[9]

Shown in Fig. 1 are typical realizations of a random velocity field obtained for both the Gaussian [left column, Figs. 1(a)–1(c)] and the modified von Kármán [right column, Figs. 1(d)–1(f)] energy spectra. Patterns of the normalized longitudinal velocity $U_{||} = u_x/c_0$ [Figs. 1(a) and 1(d)], the transverse velocity $U_{\perp} = u_y/c_0$ [Figs. 1(b) and 1(e)], and the

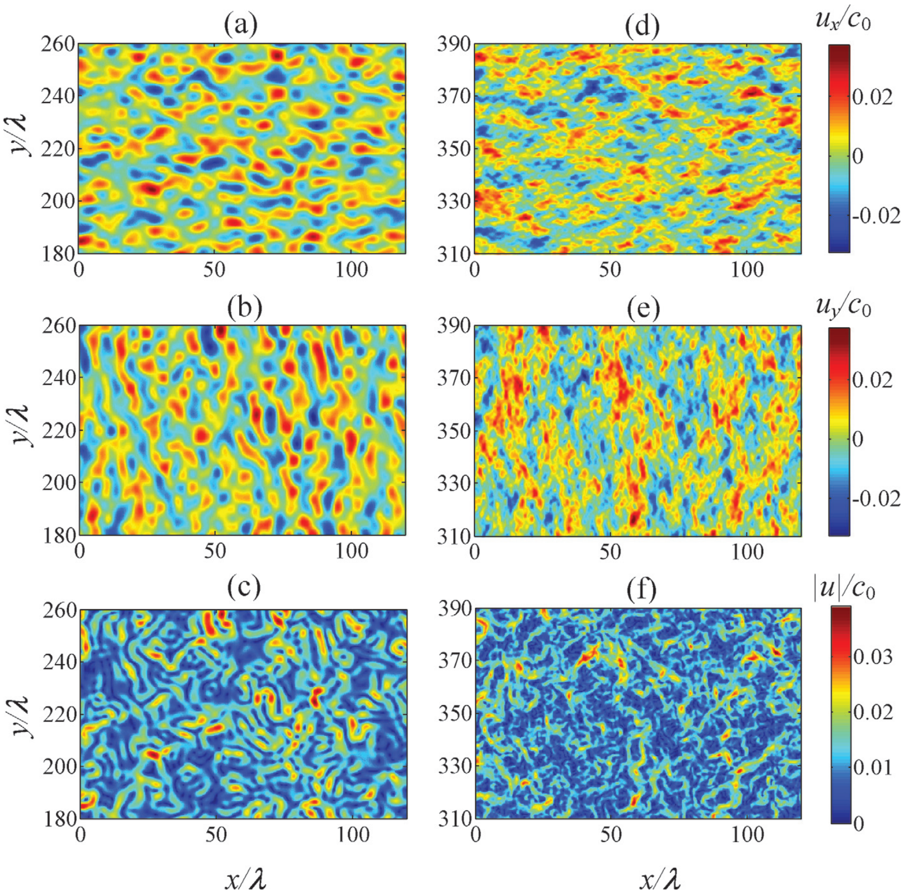

FIG. 1. (Color online) Comparison of random velocity field distributions with Gaussian (a)–(c) and modified von Kármán (d)–(f) energy spectra. (a) and (d) are longitudinal components of normalized medium velocity fluctuations, (b) and (e) are normalized transverse components, (c) and (f) are absolute values of normalized velocity fluctuations. The color bars show range of the data: velocity data has both negative and positive values and the absolute values are only positive.

absolute velocity [Figs. 1(c) and 1(f)] are presented. The velocity fluctuations with the Gaussian energy spectrum have one characteristic scale and therefore have smooth structures without small scale inclusions. In comparison, the modified von Kármán energy spectrum, with its continuum of length scales, results in much finer structure of the field. Note that the x component of the random velocity field is elongated along the x axis and y component along the y axis. This effect is in agreement with the fact that longitudinal correlation length L_f is always longer than the transverse correlation length L_g because the fluid particles move more easily in the direction of local disturbance than transverse to it. For example, in fully developed three-dimensional (3D) turbulent field the corresponding relation is: $L_f = 2L_g$ (Ref. 35).

III. NUMERICAL ALGORITHM

A. Boundary condition

An N-wave pulse was taken as the initial waveform for the simulation as it is similar to the measured sonic booms as they enter the atmospheric boundary layer.[19,36] The profile of the two shocks in the N-wave was modeled as a Taylor shock, which is the stationary solution for a plane shock wave in a thermoviscous fluid.[36,37] In dimensionless form the initial condition is expressed as

$$V_0 = \frac{\theta}{2\pi}\left[\tanh\left(\frac{N}{4A}(\theta-\pi)\right) - \tanh\left(\frac{N}{4A}(\theta+\pi)\right)\right]. \quad (11)$$

The initial waveform, modeled by Eq. (11), is consistent with two physical phenomena: nonlinearity and thermoviscous absorption. Moreover, the rise time (width) of smoothed shock is determined by the ratio between dimensionless coefficients of absorption and nonlinearity. If the rise time is defined as a time corresponding to the change in pressure on the shock from 5% to 95% of the maximum pressure, then it approximately equals to 10 A/N. In the limit of $A/N \rightarrow 0$, the initial waveform, Eq. (11), becomes an ideal N-wave with the amplitude $V_0^{\max} = 1.0$. Note, that in the case of linear wave propagation modeling ($N = 0.0$), the initial condition is taken equivalent to the case of lowest considered nonlinearity, that is, $N = 0.025$.

Rigid boundary conditions were set in transverse direction. In order to ensure that reflections from edges of numerical domain do not perturb the results, the spatial computational window was taken larger than the analyzed region. It was assumed, according to the validity limitations of the parabolic approximation, that maximum diffraction angle caused by inhomogeneity was less than 20°.[27] Thus, the spatial computational window in the transverse direction was 400λ, while the width of analyzed region was 360λ.

B. Numerical method

The nonlinear evolution equation (2) was solved using a combination of time and frequency domains based on the operator splitting procedure. The code marches in the propagation distance σ and at each grid step the equation is split in five equations describing different physical effects:

$$\text{Diffraction} \quad \frac{\partial V}{\partial \sigma} = \frac{1}{4\pi}\int \frac{\partial^2 V}{\partial \rho^2} d\theta, \tag{12}$$

$$\text{Nonlinearity} \quad \frac{\partial V}{\partial \sigma} = \frac{N}{2}\frac{\partial V^2}{\partial \theta}, \tag{13}$$

$$\text{Absorption} \quad \frac{\partial V}{\partial \sigma} = A\frac{\partial^2 V}{\partial \theta^2}, \tag{14}$$

$$\text{Axial convection} \quad \frac{\partial V}{\partial \sigma} = 2\pi U_{\parallel}\frac{\partial V}{\partial \theta}, \tag{15}$$

$$\text{Transverse convection} \quad \frac{\partial V}{\partial \sigma} = -U_{\perp}\frac{\partial V}{\partial \rho}. \tag{16}$$

The diffraction term, Eq. (12), was solved using a Crank–Nicholson finite difference (CNFD) algorithm.[38] The nonlinearity term, Eq. (13), is commonly solved using the exact implicit Poisson solution $V = V(\theta + NV\sigma)$.[38,39] This method includes linear interpolation from a nonuniform time grid back onto a uniform time grid which reduces the accuracy of the algorithm and also introduces numerical dissipation that accumulates with distance. It was shown recently that it was necessary to have about 50 grid points per shock to obtain a solution with adequate accuracy (about 3% error).[40] A very high number of grid points per pulse is therefore required in simulations as the rise time is typically very small in comparison with the pulse length. Initial rise time in model experiments of Ollivier and Blanc-Benon[22] and Lipkens and Blackstock[21] is estimated using quasi stationary solution to the Burgers equation (11) as 0.4% of the wave duration (pulse length). Taking into account total absorption (due to thermoviscous absorption and relaxation), the typical rise time value in sonic boom experiments is estimated as 1% of the wave duration, while in random foci it could be as little as 0.15% of the wave duration.[19] A requirement of 50 points per shock would require more than 10 000 grid points to model laboratory experiments and more than 30 000 grid points to model sonic booms. This result in very high memory requirements, especially in the case of 3D calculations.

In this paper, a six point explicit conservative Godunov-type algorithm of the second order of accuracy in time and first order of accuracy in propagation distance was used to model nonlinear effects.[41] This algorithm possesses good stability and good accuracy in capturing the propagation of thin shock fronts. Even with 3 temporal grid points per shock the numerical error in estimation of acoustic pulse parameters does not exceed 0.2%.[40]

At the third step, the convection in the direction of wave propagation Eq. (15) was taken into account using the exact solution for complex amplitudes C_n in the frequency domain: $V(\sigma,\rho,\theta) = \sum C_n(\sigma,\rho)\exp(-in\theta)$, $C_n(\sigma + h_\sigma,\rho) = C_n(\sigma,\rho)\exp(-i2\pi n U_{\parallel} h_\sigma)$. Here n is the harmonic number and h_σ is the grid step in propagation direction. Despite the application of forward and inverse Fourier transforms, the exact solution in the frequency domain was deemed preferable here comparing to the finite difference solution in the time domain. The frequency domain approach gave better accuracy for comparable computational time: a numerical error in the solution with three time grid points per shock was less than 1%, which was better than the accuracy achieved using the Lax–Wendroff scheme.[40,42] Moreover, this method also allows simple implementation of the exact solution for an arbitrary frequency dependent absorption and dispersion. The thermoviscous absorption term here was solved as $C_n(\sigma + h_\sigma) = C_n(\sigma)\exp(-An^2 h_\sigma)$.

Finally, at the last computational step, the convection in the direction transverse to the direction of the wave propagation Eq. (16) was taken into account. As the acoustic pressure field does not have emphasized shocks in the transverse direction, the transport equation was solved numerically using the Lax–Wendroff explicit algorithm of the second order accuracy in both spatial directions.[42]

The spatial grid steps in simulations were $h_\sigma = 2.5 \cdot 10^{-2}$ and $h_\rho = 2.0 \cdot 10^{-2}$ in longitudinal and transverse directions, respectively. The number of time grid points was $n = 1024$ per N-wave. The temporal window was padded with $2n$ points before and $4n$ points after the N-wave. The absorption was taken to be $A = 3.4 \cdot 10^{-4}$, however, this absorption was not sufficient to model fine structure of thin shocks in caustics which was controlled by the Godunov algorithm. The accuracy of simulations was tested by comparing numerical solutions calculated with different steps. The reduction of the grid steps by half resulted in less than 3% difference between the wave parameters for the two solutions.

IV. RESULTS AND DISCUSSION

A. Diffraction effects

Figure 2(a) shows the distribution of acoustic rays calculated using Eq. (3) for the realization of a turbulent atmosphere with a Gaussian energy spectrum [Figs. 1(a)–1(c)]. The figure illustrates that the random inhomogeneities result in multiple regions of acoustic ray concentration, where a corresponding local increase in pressure is expected. Propagation of an initially plane N-wave through the same random medium was also modeled using Eq. (2). Figure 2(b) shows the spatial distribution of the normalized peak positive pressure p_+/p_0 obtained in the simulations ($N = 0.05$). The peak positive pressure p_+ is defined as the maximum value of the pressure in an acoustic waveform. Overlaid are the isovelocity contour lines for the turbulent fluctuations. It can be seen that regions of peak positive pressure always follow regions where the effective sound speed $c_0 + u_x$ (gray contour lines) is low. This random focusing occurs because the regions of low sound speed act as focusing lenses distorting the phase front of the wave.[43] The peak positive pressure of the N-wave in the random foci is more than three times higher than the amplitude of the incident N-wave; however, the amplification is generally limited to propagation distances $x/\lambda < 60$. This limitation is in contrast with the results obtained for harmonic wave propagation where focusing regions occurred over all propagation distances.[18] The periodic nature of harmonic waves means that large differences in travel time cannot prevent constructive interference. However, for single pulses propagating in an inhomogeneous medium, the increasing difference in the path lengths results

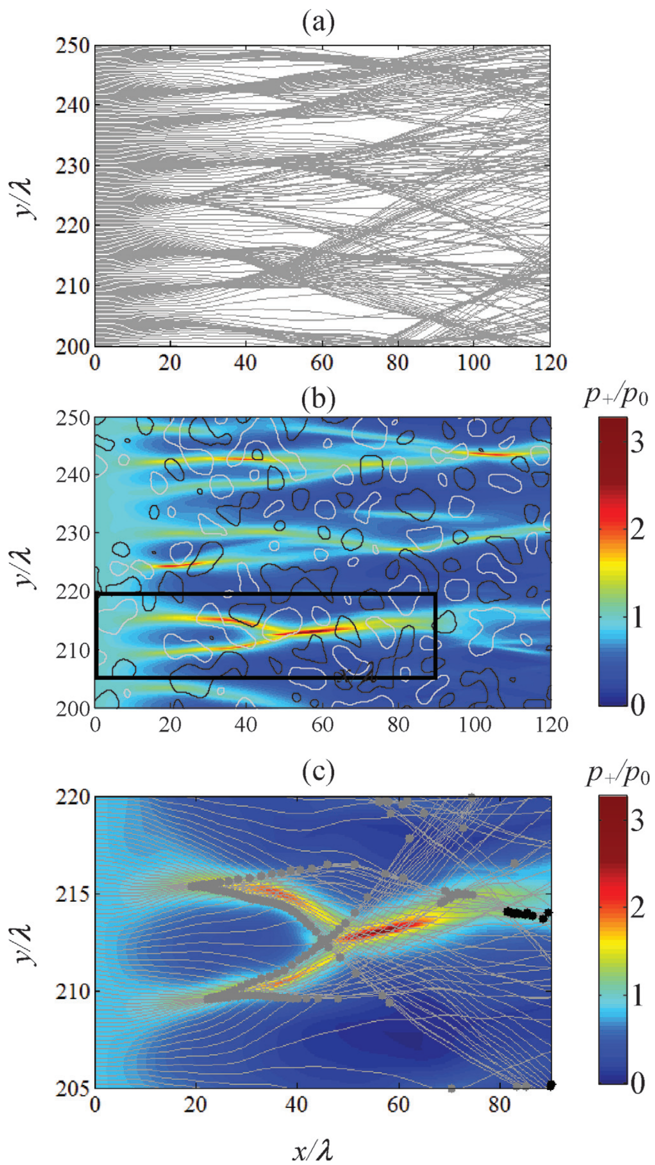

FIG. 2. (Color online) (a) acoustic ray distribution in the inhomogeneous moving medium with Gaussian energy spectrum [Figs. 1(a)–1(c)], (b) corresponding acoustic field pattern (normalized peak positive pressure p_+/p_0, $N = 0.05$) with overlaid turbulence levels: black ($u_x/c_0 = 0.009$) and gray ($u_x/c_0 = -0.009$), (c) expanded view of the peak positive pressure pattern with overlaid ray paths and caustic locations (gray points—first caustics, black points—second caustics). Area of expansion is marked with black rectangle in (b).

in the loss of coherence. For the N-wave propagation modeled here, the occurrence of high pressures far from the source is a rare event, but some relatively high pressure focusing zones are still observed even at long distances [see e.g., Fig. 2(b), $x/\lambda = 100$].

Shown in Fig. 2(c) is an expanded view of the focal region denoted by the black rectangle in Fig. 2(b). Overlaid on the peak positive pressure pattern are the ray paths (gray curves) and locations of first caustics (gray circles) and second caustics (black circles) obtained from Eq. (5). For the first caustics, the regions of ray concentration are in qualitative agreement with the high pressure levels simulated using the KZK model. However, the positions of caustics obtained in geometrical acoustics approximation, which is a high frequency limit, do not coincide with positions of maximum values of acoustic pressure. Moreover, some caustics occur in regions where the peak pressure is small. For second (and higher order) caustics, even less correlation between locations of the caustics and high pressures is observed. In addition, some focusing zones observed in the peak pressure patterns are not predicted by geometrical acoustics as they are primarily formed by the waves diffracted from the first order caustics [Fig. 2(c), $x/\lambda \sim 50$]. Diffraction effects therefore play an important role in predicting N-wave focusing through atmospheric turbulence, especially at distances beyond first caustics.

Figure 3 shows pressure waveforms obtained in simulations for the initial N-wave at various distances along the line $y/\lambda = 212$ that goes through the region of the highest peak pressure. The rounded waveform produced at $x/\lambda = 40$ is a result of defocusing; these waveforms are typical for the lower pressure regions. At $x/\lambda = 51$ the waveform has two distinct shock fronts, presumably because there are two bundles of rays that cross over at this location with slightly different travel times. The waveform at the location of the highest pressure ($x/\lambda = 55$) has a U-shape; this is consistent with the waveforms observed in the field and laboratory measurements, as well as with theoretical predictions of a waveform in a focus.[19,21,22,44,45] Steeper shock fronts are observed in the focusing zones due to higher amplitudes and therefore stronger nonlinear effects. However, nonlinear

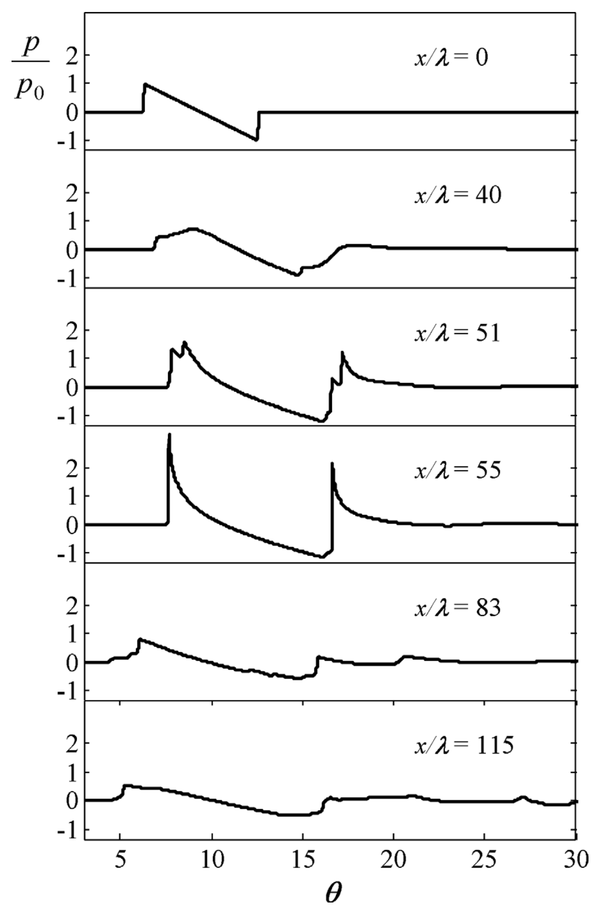

FIG. 3. Typical waveforms, simulated at various locations along the line $y/\lambda = 212$ including the source location $x/\lambda = 0$ and a caustic $x/\lambda = 55$. $N = 0.05$.

distortion of the wave (shocked structure) is also observed in regions of low level pressure due to scattering of high frequencies by the turbulence. At longer distance, $x/\lambda = 83$, the waveform is stretched over a long time frame primarily due to the large variety in travel paths through the medium. As the pulse spreads in time it becomes more unlikely for the medium to effectively refocus the wave and produce high pressures at longer distances. Increasing difference in the path lengths also results in thickening of the shock front ($x/\lambda = 115$).

B. Nonlinear effects

The effects of acoustic nonlinearity were considered by comparing numerical solutions for linear ($N = 0$) and nonlinear ($N = 0.025$ and $N = 0.05$) wave propagation. Figure 4(a) shows the peak pressure as a function of propagation distance along the line $y/\lambda = 212$, the same line as for the waveforms shown in Fig. 3. An initial decay of the peak pressure while propagating in the defocusing region is observed for all three cases: linear and nonlinear propagation. However, in the vicinity of the caustic nonlinear effects result in more effective focusing with the highest 60% increase of the gain in pressure for $N = 0.05$ in comparison with the linear one. The locations of the pressure maxima for nonlinear waves are shifted a few wavelengths in the longitudinal direction due to a combination of nonlinear defocusing and nonlinear dissipation effects. For $N = 0.025$ nonlinear defocusing is dominant and the focus shifts the furthest at $x/\lambda = 56.1$. For stronger nonlinearity ($N = 0.05$), dissipation at the shock front results in a slight shift of the focus ($x/\lambda = 55.3$) back toward the linear peak ($x/\lambda = 53.7$). The focal spot becomes shorter in the axial direction for stronger nonlinearity which is consistent with tighter focusing of signals containing steeper shocks, i.e. higher frequencies.

Figure 4(b) shows the peak positive pressure as a function of the transverse coordinate at $x/\lambda = 55$. Simulations with higher nonlinearity yield narrower focal spots (half amplitude width is λ for $N = 0.05$, 2λ for $N = 0.025$, and 3λ for the linear case), which is also consistent with better focusing of high frequency components generated due to nonlinear propagation. The shift of the peak pressure in the transverse direction is negligible as nonlinear refraction and dissipation effects act in the propagation direction, which remain primarily along the x axis.

The evolution of the maximum value of peak positive pressure p_{max} as a function of propagation distance is shown in Fig. 4(c). Here, p_{max} is defined as the maximum value of p_+ from all waveforms in the transverse direction between $y/\lambda = 20$ and $y/\lambda = 380$. The linear and nonlinear propagation curves are very similar up to distances of $x/\lambda = 20$. Beyond this range, the maximum peak pressure is almost always higher for nonlinear propagation, i.e., nonlinearity enhances focusing. However, the dependence of focusing efficiency on nonlinearity parameter is not monotonic. Initial increase of nonlinearity from $N = 0$ results in higher pressure focusing gain. At some "critical" point the growth of focal gain with nonlinearity switches to the decay, as nonlinear dissipation at the shock front and nonlinear refraction become dominant over focusing effects. Strong nonlinearity ($N = 0.05$) results in lower level of maximum pressure than moderate nonlinearity ($N = 0.025$) at most distances.

In general, nonlinearity will enhance focusing of an acoustic wave in randomly inhomogeneous medium only if the characteristic nonlinear distance x_n is shorter than the distance of the first caustic formation: x_{caust}. In other words, if the peak pressure decrease due to nonlinear dissipation is excessive before a caustic forms, then the ability of

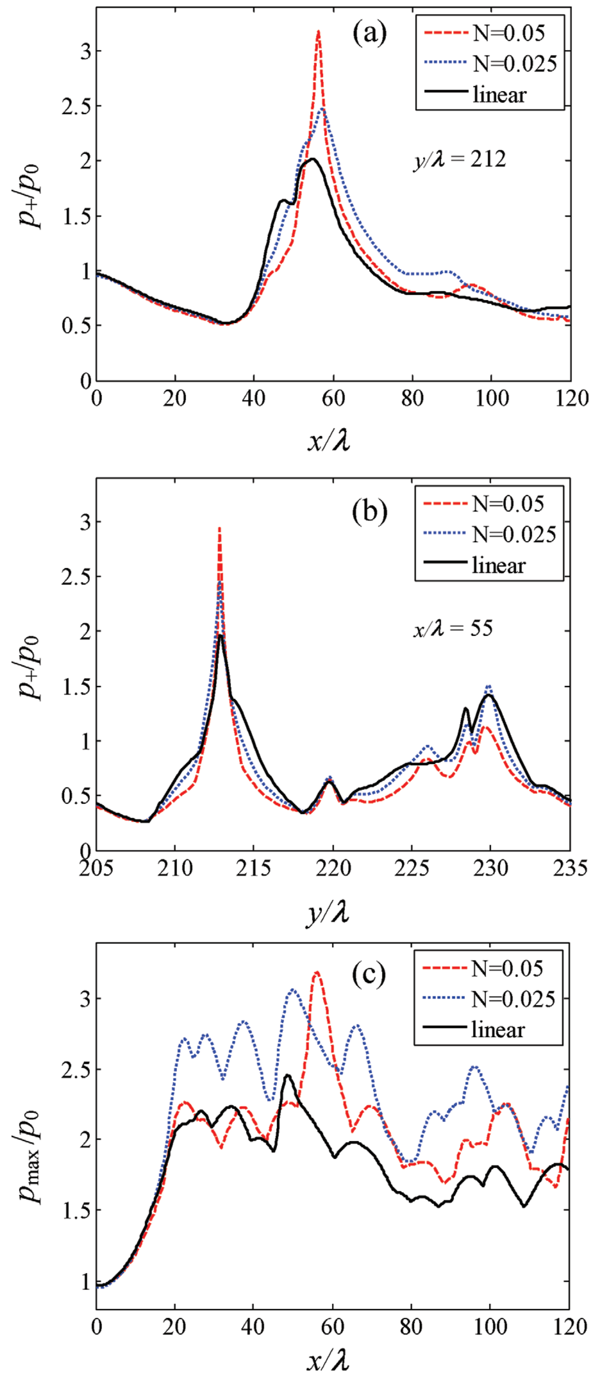

FIG. 4. (Color online) Peak positive pressure distribution along (a) the horizontal line $y/\lambda = 212$, (b) the vertical line $x/\lambda = 55$; (c) maximum value of peak positive pressure, p_{max}, calculated from all waveforms in the lateral direction along the horizontal axis. Data are shown for $N = 0$ (solid curve), $N = 0.025$ (dotted curve) and $N = 0.05$ (dashed curve).

nonlinearity to enhance focusing is diminished. The distance where the probability density of the occurrence of first caustic has a maximum can be determined in geometrical acoustics approximation, from the root mean square velocity of fluctuations σ_u, and the characteristic scale L of the inhomogeneities.[6] For the random medium considered here,

$$x_{\text{caust}} = 0.28L(c_0/\sigma_u)^{2/3}. \quad (17)$$

According to Eq. (17) for $N = 0.025$ the nonlinear distance $x_n/\lambda = 40$ is longer than the caustic formation distance $x_{\text{caust}}/\lambda = 26$ ($x_n > x_{\text{caust}}$) and thus nonlinearity enhances focusing in the caustics. For $N = 0.05$ the nonlinear distance is $x_n/\lambda = 20$ which is less than the distance to the first caustics ($x_n < x_{\text{caust}}$) and therefore nonlinear dissipation suppresses nonlinear enhancement observed for $N = 0.025$. However, this rule is valid only on average; there is still a chance to observe better focusing for strong nonlinearities. For example, the local pressure maximum formed due to constructive interference of the two bundles of rays [Fig. 2(c)] at the distance $x/\lambda = 55$ is higher for $N = 0.05$ than for $N = 0.025$. Another phenomenon that can be observed is that the positions of the peak pressure maxima in Fig. 4(c) vary with the different values of N for distances beyond the caustic formation distance. This indicates that peak pressures are sensitive to interplay between nonlinearity, diffraction, and inhomogeneities.

The effect of nonlinearity on waveform distortion is shown in Fig. 5, where waveforms simulated at different points of the acoustic field are presented.

In the focal point [Fig. 5(a)] the N-wave transforms into a classical U-shaped waveform, which occurs because focusing manifests itself as a differentiation. As a result of the differentiation, the peak amplitude of the U-wave increases for N-waves with thinner shock fronts. The peak positive pressure of the U-wave in the nonlinear case ($N = 0.05$) is more than 60% higher than its value in the linear case as nonlinearity results in steepening of the shock front, which in nonlinear case is more than 30 times steeper than in the linear one. However, in regions of low pressure, the amplitude of nonlinear wave may be lower than that of the linear one [Figs. 5(c) and 5(d)] due to nonlinear dissipation. Because of scattering of higher harmonics by caustics, steep shocks are observed even in shadow zones where pressure amplitude is low [Fig. 5(c)]. At longer propagation distances both linear and nonlinear waveforms have very long tails as inhomogeneities introduce multiple paths with different times of flight. In some cases, due to superposition of diffracted waves, it is possible for the pressure in the tail to exceed the pressure of the main wave and to form a relatively thin shock [Fig. 5(d)]. Generally, the tail of the wave is longer outside focusing regions than for U-waves inside them. For all waveforms, nonlinear effects result in steepening of the shock front and lengthening of the pulse duration. However, in spite of nonlinear steepening, waveforms in shadow zones have thicker shock fronts than the initial waveform, apparently due to the influence of inhomogeneities.

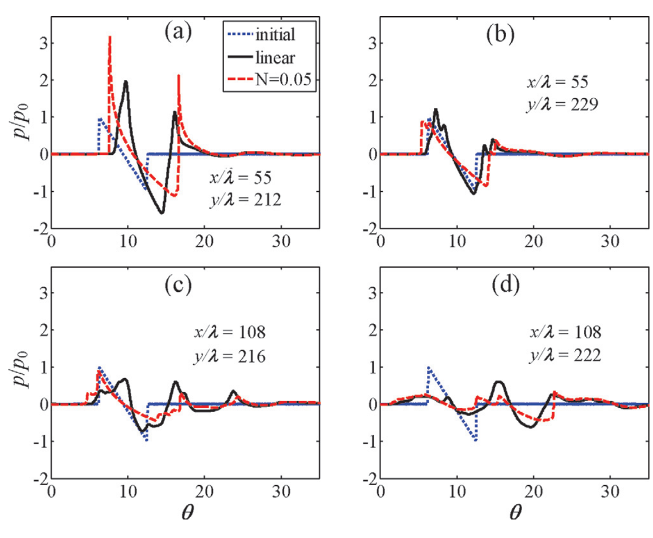

FIG. 5. (Color online) Typical linear ($N = 0$) and nonlinear ($N = 0.05$) waveforms simulated at different points of the acoustic pressure pattern including (a) focal zones and (b)–(d) shadow areas.

C. Effect of random inhomogeneities on *N*-wave statistics

The statistics of N-waves were calculated by analyzing waveforms from a single very large realization. The ergodicity hypothesis was invoked so that calculating statistics across the simulations was equivalent to doing calculations of many realizations. The ergodic property was checked by changing the width of the simulation from 50 L_0 to 100 L_0 and confirming that the mean parameter values did not change. Figure 6 shows the evolution of N-wave metrics with propagation distance. Shown in the left column are mean peak positive pressure $\langle p_+/p_0\rangle$(a), mean rise time $\langle\theta_{sh}\rangle$(c), and mean arrival time shift $\langle\Delta\theta\rangle$(e). The shift in arrival time was defined as a difference between time-of-flight for a simulation in a turbulent atmosphere and the time-of-flight for the case of linear propagation in a still medium. The time-of-flight of the pulse was calculated at the 10% level of the maximum pulse pressure. The right column shows the corresponding standard deviations. Data are shown for both linear ($N = 0$) and nonlinear ($N = 0.05$) propagation in the turbulent (dashed curves) and still (solid curves) media.

In the turbulent medium, up to $x/\lambda \simeq 15$, the mean wave characteristics behave as if there was no turbulence at all. The mean peak pressure decreases more rapidly for the nonlinear case due to nonlinear dissipation [Fig. 6(a)]. For both linear and nonlinear propagation, the difference in mean peak pressure in still and turbulent media becomes notable for $x/\lambda > 15$ and achieves its local maximum approximately at the location of the first order caustic formation $(x/\lambda)_{\text{caust}} = 26$.

A gradual decay of the mean peak pressure with distance follows the geometry of acoustic field in the turbulent medium. The field consists of localized focusing regions with high pressure and larger defocusing regions with lower pressure. The probability to observe low pressures is therefore higher and as a result the mean peak pressure diminishes. The standard deviation of the peak pressure [Fig. 6(b)]

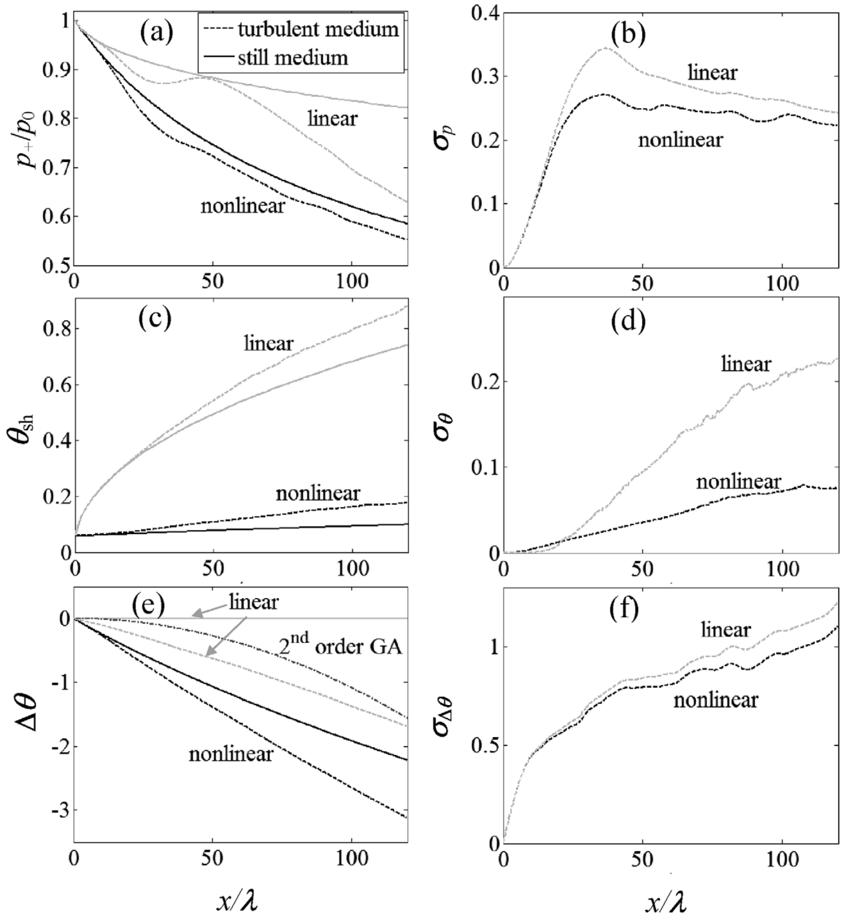

FIG. 6. Evolution of N-wave metrics with propagation distance in turbulent (dashed) and still (solid) media for linear $N=0$ and nonlinear $N=0.05$ regimes. The left column displays (a) mean peak positive pressure, (c) mean rise time, and (e) mean arrival time shift. The right column shows the corresponding standard deviations. The dashed–dotted line shows the second order approximation for the mean arrival time obtained within the geometrical acoustics model.

increases almost linearly up to the distance of the first caustic formation and then decreases slowly. This monotonic decrease is due to the fact that effective refocusing of the pulse at long distances is a rare phenomenon and peak pressures observed in random foci are smaller than at the distance of first caustics.

The mean rise time and its standard deviation, Figs. 6(c) and 6(d), increase monotonically with propagation distance for all cases. For distances $x > x_{\text{caust}}$ the presence of turbulence results in a longer mean rise time than in the still medium because multiple arrivals of the scattered waves affect the coherence needed for a short rise time. A greater increase in the rise time is observed in the linear case because when nonlinearity is present it steepens the waveform and prevents the shock rise time from increasing too much. However, on average, nonlinearity cannot compensate completely for the effects of turbulence. The standard deviation of the rise time in nonlinear turbulent medium is of the same order as its mean value, thus some of the waveforms have a rise time less than the initial one.

As shown in Fig. 6(e), the presence of inhomogeneities results, on average, in a faster arrival time of the pulse. This is consistent with the principle of least action or the Fermat principle in application to acoustics: the wave path minimizes travel time of the wave. For example, linear geometrical acoustics gives faster arrivals only when second order effects – ray bending are taken into account.[46] The analytical solution for $\langle\Delta\theta\rangle$ at second order in a 2D Cartesian random field with Gaussian energy spectrum is $\langle\Delta\theta\rangle = -\pi^{3/2}\sigma^2(\sigma_u/c_0)^2/L$, i.e., the mean arrival time decreases quadratically with propagation distance [Fig. 6(e), dashed–dotted line]. In contrast, the diffraction model employed here accounts for the first order effect and yields almost linear decrease of the mean arrival time. Such behavior of arrival time was also observed in analytical solutions obtained from the parabolic equation using the Rytov approximation.[47] Nonlinear lengthening of the pulse results in even earlier arrivals. However, the difference in arrival time in still and turbulent media is greater for the linear propagation. For example, at the distance $x/\lambda = 120$ the difference $\langle\Delta\theta\rangle_{\text{lin}} - \langle\Delta\theta\rangle_{\text{lin}}^{\text{turb}} = -1.7$ for the linear case and $\langle\Delta\theta\rangle_{\text{nl}} - \langle\Delta\theta\rangle_{\text{nl}}^{\text{turb}} = -0.9$ for the nonlinear case. Nonlinearity thus decreases the effect of turbulence on arrival time here by a factor of two. This shows the significance of nonlinear and diffraction effects on arrival time.

Probability density distributions of the peak positive pressure in a nonlinear ($N=0.05$) turbulent medium are presented in Fig. 7(a) at different propagation distances. All distributions are scaled between the minimum and maximum observed values of the peak pressure. It can be seen that initially narrow probability distribution becomes wider with propagation distance. The maximum of the distribution translates to lower pressures that are always smaller than the corresponding mean value. The high pressure tail in the distribution exceeds by three-fold the value of the initial peak pressure. Although the distribution itself shifts to lower peak pressure, a few occurrences of high amplitude N-waves still exist. For example, at the distance $x/\lambda = 60$ the probability of a normalized pressure amplitude greater than 1.5 is 1.3% and the pressure more than doubles with a probability of 0.2%.

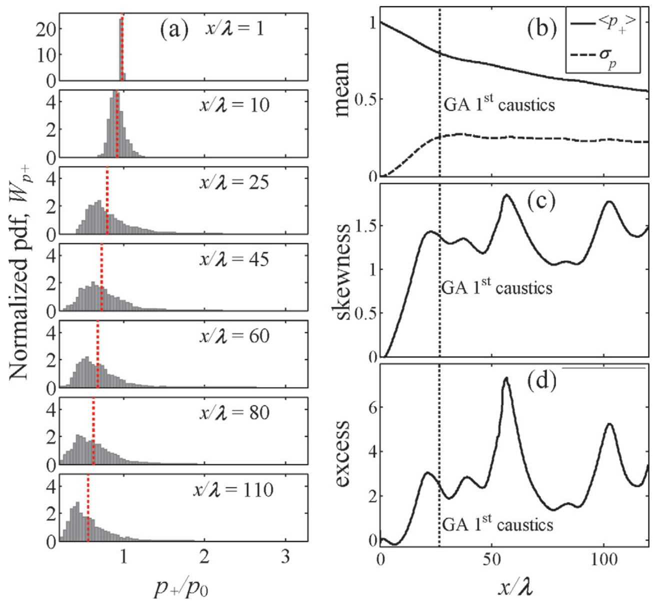

FIG. 7. (Color online) (a) Normalized probability density distributions of the peak positive pressure at different distances from the source for nonlinear ($N = 0.05$) propagation in a turbulent atmosphere. The bin width is 0.038 and the vertical dotted line denotes the mean value. Distribution parameters versus propagation distance are shown in the right column: (b) mean peak positive pressure and its standard deviation, (c) skewness, (d) excess factor. The vertical dotted line indicates the distance of the first caustic formation obtained in the geometrical acoustics approximation.

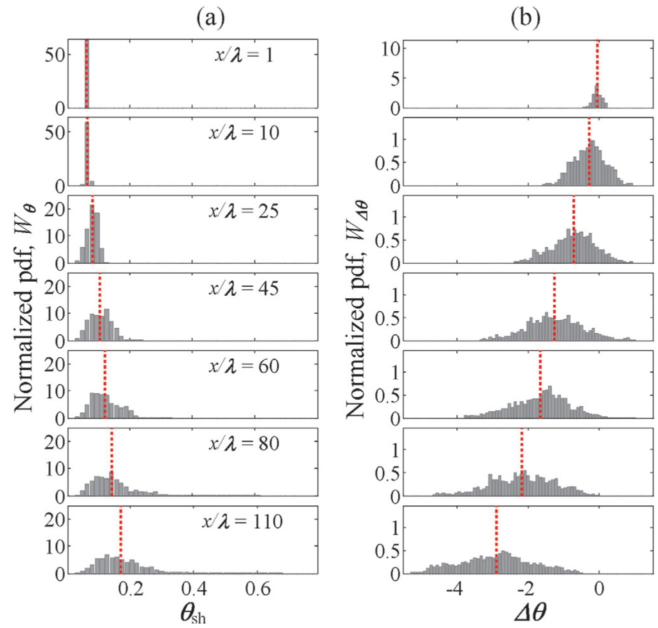

FIG. 8. (Color online) Normalized probability density distributions at different distances from the source for nonlinear propagation ($N = 0.05$) in a turbulent atmosphere. (a) Shock front rise time (bin width 0.016), (b) arrival time shift (bin width 0.09). The vertical dotted line denotes the mean value.

Figures 7(b)–7(d) show the first four moments of the peak positive pressure distribution along the propagation coordinate: mean value, standard deviation, skewness, and excess factor. The skewness is a measure of the asymmetry of a given distribution as compared to the Gaussian one. If it is positive, the right-hand side of the distribution contains more values than its left-hand side. The excess factor gives a relative measure of "peakedness" of the distribution. A high excess value means that more of the variance is due to the infrequent extreme deviations, as opposed to the frequent modestly sized deviations. Standard deviation, skewness, and excess factors should increase at the distances where the wave is most probable to focus. At these distances the distribution of the peak pressure becomes asymmetric showing occurrence of infrequent extreme fluctuations. Indeed, all the factors, except the mean value, grow rapidly from zero to some characteristic value attained at the distance where geometrical acoustics predicts formation of the first caustics: vertical lines in Fig. 7 as given by Eq. (17). Up to the first caustics the propagation is well described by the geometrical acoustics. In contrast to the high order factors, the mean peak positive pressure is not significantly affected by the occurrence of the first and higher order caustics [Fig. 7(b)]. At longer distances the standard deviation saturates, but the skewness and excess factor are subjected to a strong change as the wave propagates through the randomly inhomogeneous medium. The strongest fluctuations correspond to the most intense focusing of the wave. For example, both the skewness and the excess factor peak at the distance $x/\lambda = 60$ corresponding to the focusing coefficient $p_+/p_0 = 3.2$. The peaks are also situated at the distance $x/\lambda = 105$ from the source where the second order caustics occur—the black dots shown in Fig. 2.

Figure 8(a) shows the probability density distributions of the rise time calculated at different distances. The maximum of the distribution moves toward higher values with the propagation distance. This is consistent with the corresponding shift to the lower pressures in the distribution of the mean peak positive pressure [Fig. 7(a)] as the rise time for lower amplitude shocks in nonlinear medium is longer. Nevertheless, very short rise times are also observed. For example, in the focusing region $x/\lambda = 60$ the probability of a decrease in rise time comparing to its initial value is 3.4%. The minimum rise time observed is $\theta_{sh} = 0.022$, which is almost three times smaller than the initial one.

The probability density distributions for the arrival time [Fig. 8(b)] show that both the maximum of the distribution and the mean value shift to earlier time and that this shifts increase with propagation distance in a similar manner. Earlier arrivals up to $\Delta\theta = -5.25$, more than 3/4 of the initial N-wave duration, are predicted. The distribution also becomes wider with the distance.

D. Effect of turbulence model

The propagation of N-waves in a single-scale inhomogeneous medium with a Gaussian energy spectrum was studied in the previous sections. Here we consider a more realistic turbulent field which is a multiscale randomly inhomogeneous moving medium with a modified von Kármán spectrum. Figure 9(a) shows the distribution of the peak pressure of the initial N-wave propagating through the turbulent field given in Figs. 1(d)–1(f). Overlaid are contour levels of the

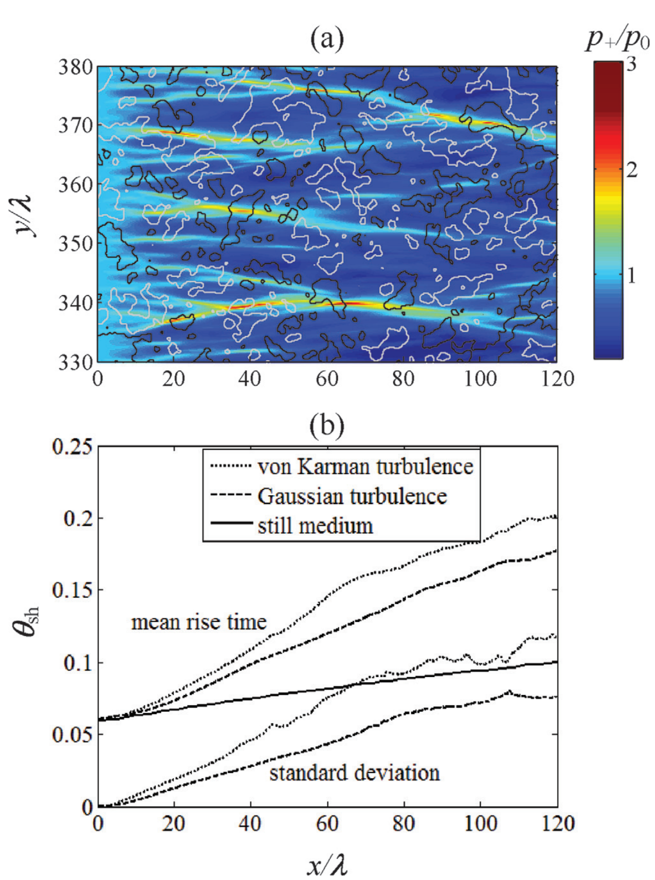

FIG. 9. (Color online) (a) Peak positive pressure distribution ($N = 0.05$) in a randomly inhomogeneous field with a modified von Kármán energy spectrum [Figs. 1(d)–1(f)]. Levels of turbulence intensity are marked with black ($u_x/c_0 = 0.009$) and gray ($u_x/c_0 = -0.009$) contours. (b) The mean rise time and standard deviation along the propagation coordinate in a random medium with Gaussian (dashed) and modified von Kármán (dotted) energy spectra. Solid curve—mean rise time in a still medium.

longitudinal component of the random velocity field. Multiple focusing and defocusing zones of the acoustic wave are observed similar to the turbulence with Gaussian spectrum. Focusing zones follow areas of low effective sound speed and defocusing zones follow areas of high effective sound speed. However, as expected, the structure of the acoustic field is more complex and has fine structure due to the presence of small scale velocity fluctuations.[31] Moreover, multiscale inhomogeneities result in occurrence of the first focusing zones at shorter distances.[6]

The effect of the modified von Kármán spectrum on the statistics of the peak positive pressure and arrival time of the acoustic wave was found to be both qualitatively and quantitatively analogous to that given by the Gaussian spectrum. The most significant difference was obtained for the rise time of the wave. Figure 9(b) shows the mean rise time and its standard deviation along the propagation coordinate for a modified von Kármán spectrum (dotted curves), Gaussian spectrum (dashed curves), and still medium (solid curve). The increase in the rise time in the still medium is due to the combined effect of nonlinear dissipation ($N = 0.05$) at the shock and thermoviscous absorption, both decreasing the pressure and increasing the rise time. When comparing the two random fields it can be seen that the modified von Kármán spectrum results in a longer shock rise time and a higher standard deviations than the Gaussian spectrum. This suggests that the shock front rise time is most sensitive to small scale inhomogeneities in the turbulent field.

E. Effect of the transverse velocity component

The KZK-type Eq. (2) contains a term, which accounts for the transverse component of the velocity field. To estimate the effect of this component of vectorial fluctuations on the acoustic field, two types of computation were performed: one which accounted for both longitudinal and transverse fluctuations and the other that accounted only for the longitudinal component. The simulations were performed for the random velocity field with the modified von Kármán energy spectrum and the results for the peak positive pressure along both the propagation axis and the lateral axis are shown in Fig. 10. Very little difference is seen between the curves in either axis. The presence of lateral velocity fluctuations results in slight transverse shifting of the focal regions and small changes in focusing efficiency. The shifts in foci locations do not exceed half a wavelength and the change in peak pressure in focusing zones is less than 3%. The results suggest that the acoustic field is insensitive to lateral velocity fluctuations for the turbulence model considered here. This is in agreement with the fact that in Eq. (1) the term which accounts for the transverse velocity fluctuations is smaller than the term which accounts for longitudinal velocity fluctuations.[1,18] However, for large scale fluctuations or lateral fluctuating flow, the effect can be significant.[18]

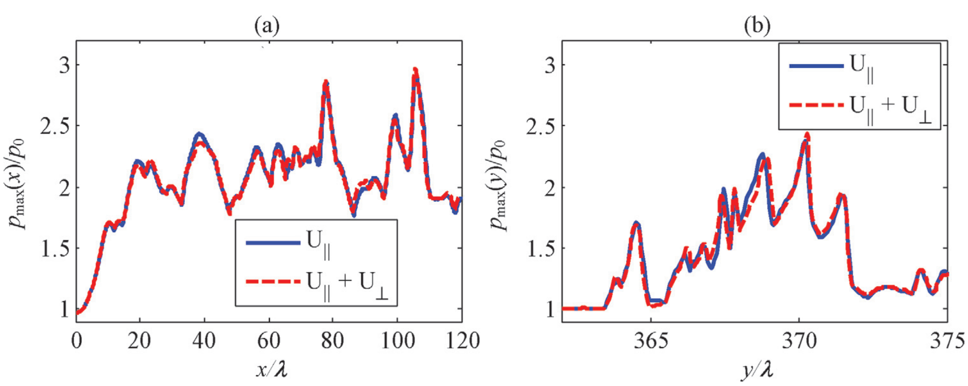

FIG. 10. (Color online) Distributions of the peak positive pressure calculated with or without account for the transverse component of the random velocity field with the modified von Kármán spectrum. (a) The maximum value as a function of propagation distance where the maximum value at each distance x was determined from all waveforms in the lateral (y) axis and (b) the maximum value as a function of lateral distance based on all waveforms in the propagation (x) axis.

V. CONCLUSION

A generalized KZK-type evolution equation in 2D Cartesian geometry was applied to study the propagation of high amplitude acoustic pulses in randomly inhomogeneous media. The model of random Fourier modes was used to generate single and multiscale turbulent velocity fields with Gaussian and modified von Kármán energy spectra. The advance made here is that the nonlinear propagation of *N*-waves in a turbulent medium was studied with account for both longitudinal and lateral components of the flow. The influence of random focusing of *N*-waves on the statistics of the peak positive pressure, shock rise time, and arrival times of the waves was investigated.

Nonlinear *N*-wave propagation in a random moving media was modeled using a split-step marching algorithm. The numerical procedure for each physical term was optimized to provide a good accuracy and reasonable computational time. In particular, a Godunov scheme for the nonlinear term was employed that gave better resolution of the shock front and resulted in less computational time in comparison with the exact implicit solution of the widely used Texas algorithm.[38] Calculation of the term governing longitudinal inhomogeneities based on the exact solution in the frequency domain also provided much better accuracy with negligible increase in computation time as compared with the direct finite difference time-domain modeling.

Results of simulations showed the importance of diffraction phenomena to capture the effects induced by the atmospheric turbulence. Qualitative and quantitative differences with results obtained using geometrical acoustics approximation were demonstrated for locations of focusing regions, especially at distances beyond formation of the first caustics $x > x_{\mathrm{caust}}$.

The simulated waveforms were consistent with those measured for sonic boom propagation through the atmospheric boundary layer. For example, the *U*-shaped waveforms with high amplitudes and short rise times that occur because of local focusing by turbulence inhomogeneities and increase the perceived annoyance of the boom were predicted in focal regions. Note, that shocks were obtained even in regions of low pressure due to scattering of high harmonics on caustics. It was shown that acoustic nonlinearity enhances local focusing effects, increasing the peak pressure (up to 60%) and decreasing the rise time (more than 30 times in random foci). With further increase of nonlinearity strong nonlinear dissipation suppressed waveforms before the foci and the peak pressure increase was reduced but was still greater than in the linear case. Nonlinear refraction shifted foci locations further from the source.

Statistical analysis of nonlinear ($N = 0.05$) acoustic field showed that at distances $x > x_{\mathrm{caust}}$ the presence of the turbulence resulted in changes to the pressure (up to five times increase in the peak values but a 6% decrease in the mean), to the rise time of the shock front (twofold increase of the mean), and to the average time-of-flight (faster average arrival on about 15% of the initial pulse duration) as compared to those parameters calculated in a motionless medium. Nonlinear effects were shown to decrease the effect of random inhomogeneities on the mean characteristics of the *N*-wave but were not sufficient for complete compensation. Note, that the first order effects of random inhomogeneities on the mean arrival time were captured by the model, while geometrical acoustics gave only the second order effects.

The choice of the turbulence model had a small impact on the predictions of mean peak positive pressure and arrival time. These parameters were mainly determined by large scale inhomogeneities. In contrast, mean rise time was equally affected by both large and small scales of turbulent fluctuations.

The presence of a transverse flow was also negligible for the turbulence model used here. The structure of the acoustic field in turbulent flow was determined by its longitudinal component. However the effect of transverse flow becomes more pronounced with increase of the inhomogeneity scale, especially for uniform transverse flows.[18] This suggests that transverse fluctuations of random velocity fields should be accounted for in models that wish to correctly predict peak and mean characteristics of the acoustic field.

Finally, the simulation code developed here has the potential to assess the impact of atmospheric turbulence on sonic boom propagation in order to determine the effect and the frequency of highly disturbing events. It could also be employed to investigate jet-noise and other high amplitude sound in the atmosphere.

ACKNOWLEDGMENTS

This work was supported by the Russian Foundation for Basic Research 10-02-91062/Centre National de la Recherche Scientifique 5063 Projet International de Coopération Scientifique grant. Computer simulations were performed using "Chebyshev" SKIF-Moscow State University (MSU) supercomputer complex. The authors are thankful to Dr. Oleg Sapozhnikov for fruitful scientific discussions.

[1] V.E. Ostashev, *Acoustics in Moving Inhomogeneous Media* (Ed. E&Fn Spon, London, 1997), pp. 27–89.
[2] V.I. Tatarskii, *The Effects of the Turbulent Atmosphere on Wave Propagation* (Israel Program for Scientific Translations, Jerusalem, 1971), pp. 198–213.
[3] V.A. Krasilnikov, "Linear and nonlinear sound propagation in turbulent and inhomogeneous media," Acoust. Phys. **44**, 481–490 (1998).
[4] A.D. Pierce, "Statistical theory of atmospheric turbulence effects on sonic-boom rise times," J. Acoust. Soc. Am. **49**, 906–924 (1971).
[5] V.A. Kulkarny, and B.S. White, "Focusing of waves in turbulent inhomogeneous media," Phys. Fluids **25**, 1770–1784 (1982).
[6] P. Blanc-Benon, D. Juvé, and G. Comte-Bellot, "Occurrence of caustics for high-frequency acoustic waves propagating through turbulent fields," Theor. Comput. Fluid Dyn. **2**, 271–278 (1991).
[7] O.V. Rudenko, A.K. Sukhorukova, and A.P. Sukhorukov, "Full solutions to equations of geometrical acoustics in stratified moving media," Acoust. Phys. **43**, 339–343 (1997).
[8] V. Ostashev, D. Juvé, and Ph. Blanc-Benon, "Derivation of a wide-angle parabolic equation for sound waves in inhomogeneous moving media," Acta Acust. Acust. **83**, 455–460 (1997).
[9] L. Dallois, Ph. Blanc-Benon, and D. Juvé, "A wide-angle parabolic equation for acoustic waves in inhomogeneous moving media: Applications to atmospheric sound propagation," J. Comput. Acoust. **9**(2), 477–494 (2001).
[10] O.A. Godin, "Wide-angle parabolic equations for sound in a 3D inhomogeneous moving medium," Phys. Dokl. **47**, 643–646 (2002).

[11]M. Kelly, R. Raspet, and H.E. Bass, "Scattering of sonic booms by anisotropic turbulence in the atmosphere," J. Acoust. Soc. Am. **107**, 3059–3064 (2000).
[12]A.A. Piacsek, "Atmospheric turbulence conditions leading to focused and folded sonic boom wavefronts," J. Acoust. Soc. Am. **111**, 520–529 (2002).
[13]R. Marchiano, F. Coulouvrat, and J.-L. Thomas, "Nonlinear focusing of acoustic shock waves at a caustic cusp," J. Acoust. Soc. Am. **117**, 566–577 (2005).
[14]P.V. Yuldashev, N.A. Bryseva, M.V. Averiyanov, P. Blanc-Benon, and V.A. Khokhlova, "Statistical properties of nonlinear diffracting *N*-wave behind a random phase screen," Acoust. Phys. **56**(2), 158–167 (2010).
[15]L. Ganjehi, R. Marchiano, F. Coulouvrat, and J.-L. Thomas, "Evidence of wave front folding of sonic booms by a laboratory-scale deterministic experiment of shock waves in a heterogeneous medium," J. Acoust. Soc. Am. **124**, 57–71 (2008).
[16]Y. Jing, and R.O. Cleveland, "Modeling the propagation of nonlinear three-dimensional acoustic beams in inhomogeneous media," J. Acoust. Soc. Am. **122**, 1352–1364 (2007).
[17]P. Blanc-Benon, B. Lipkens, L. Dallois, M.F. Hamilton, and D.T. Blackstock, "Propagation of finite amplitude sound through turbulence: Modeling with geometrical acoustics and the parabolic approximation," J. Acoust. Soc. Am. **111**, 487–498 (2002).
[18]M. V. Aver'yanov, V.A. Khokhlova, O.A. Sapozhnikov, P. Blanc-Benon, and R.O. Cleveland, "Parabolic equation for nonlinear acoustic wave propagation in inhomogeneous moving media," Acoust. Phys. **52**, 623–632 (2006).
[19]R.A. Lee and J.M. Downing, "Sonic booms produced by US Air Force and US Navy aircraft: Measured data," Technical Report (1991).
[20]D.J. Maglieri, "Some effects of airplane operations and the atmosphere on sonic-boom signatures," J. Acoust. Soc. Am. **39**, S36–S42 (1966).
[21]B. Lipkens and D.T. Blackstock, "Model experiment to study sonic boom propagation through turbulence. Part I: Model experiment and general results," J. Acoust. Soc. Am. **103**, 148–158 (1998).
[22]S. Ollivier, and P. Blanc-Benon, "Model experiment to study acoustic *N*-wave propagation through turbulence," in *Proceedings of 10th AIAA/CEAS Aeroacoustics Conference,* AIAA2004-2921 paper (Manchester, UK, 2004).
[23]A. Niedzwiecki and H.S. Ribner, "Subjective loudness of sonic-boom: N-wave and minimized (low-boom) signatures," J. Acoust. Soc. Am. **64**, 1622 (1978).
[24]D.J. Maglieri and H.W. Carlson, "The shock wave noise problem of supersonic aircraft in steady flight," Technical Report, NASA-MEMO-3-4-59L (1959).
[25]J.D. Leatherwood, B.M. Sullivan, K.P. Shepherd, D.A. McCurdy, and S.A. Brown, "Summary of recent NASA studies of human response to sonic booms," J. Acoust. Soc. Am. **111**, 586–598 (2002).
[26]R. Blumrich, F. Coulouvrat, and D. Heimann, "Variability of focused sonic booms from accelerating supersonic aircraft in consideration of meteorological effects," J. Acoust. Soc. Am. **118**, 696–706 (2005).
[27]J. N. Tjötta, S. Tjötta, and E.H. Vefring, "Effects of focusing on the nonlinear interaction between two collinear finite amplitude sound beams," J. Acoust. Soc. Am. **89**, 1017–1027 (1991).
[28]H.E. Bass, J. Ezell, and R. Raspet, "Effect of vibrational relaxation on rise times of shock waves in the atmosphere," J. Acoust. Soc. Am. **74**, 1514–1517 (1983).
[29]D.I. Blokhintsev, *Acoustics of a Nonhomogeneous Moving Medium* (Science. Engl. transl.: NASA Tech. Memorandum 1399, Moscow, 1956), pp. 1–74 (1946).
[30]S.M. Candel, "Numerical solution of conservation equations arising in linear wave theory—Application to aeroacoustics," J. Fluid Mech. **83**, 465–493 (1977).
[31]K. Wert, P. Blanc-Benon, and D. Juvé, "Effect of turbulence scale resolution on numerical simulation of atmospheric sound propagation," in *Proceedings of 4th AIAA/CEAS Aeroacoustics Conference*, AIAA1998-2245 Toulouse, paper (1998).
[32]D.K. Wilson, "A turbulence spectral model for sound propagation in the atmosphere that incorporates shear and buoyancy forcings," J. Acoust. Soc. Am. **108**, 2021–2038 (2000).
[33]R. Frehlich, Y. Meillier, M.L. Jensen, B. Balsley, and R. Sharman, "Measurements of boundary layer profiles in an urban environment," J. Appl. Meteorol. Climatol. **45**, 821–837 (2006).
[34]I. Smalikho, F. Köpp, and R. Rham, "Measurement of atmospheric turbulence by 2-μm Doppler Lidar," J. Atmos. Ocean. Technol. **22**, 1733–1747 (2005).
[35]G. Comte-Bellot and C. Bailly, *Turbulence* (CNRS, France, 2003), pp. 133–183.
[36]O.V. Rudenko and S.I. Soluyan, *Theoretical Foundations of Nonlinear Acoustics* (Consultants Bureau, New York, 1977), pp. 42–65.
[37]A.D. Pierce, *Acoustics: An Introduction to Its Physical Principles and Applications* (McGraw-Hill Book Co., New York, 1981), pp. 566–619.
[38]Y.S. Lee and M.F. Hamilton, "Time-domain modeling of pulsed finite-amplitude sound beams," J. Acoust. Soc. Am. **97**(2), 906–917 (1995).
[39]R.O. Cleveland, J.P. Chambers, H.E. Bass, R. Raspet, D.T. Blackstock, and M.F. Hamilton, "Comparison of computer codes for the propagation of sonic boom waveforms through isothermal atmospheres," J. Acoust. Soc. Am. **100**, 3017–3027 (1996).
[40]M.V. Averiyanov, "Nonlinear-diffraction effects in propagation of sound waves through turbulent atmosphere: experimental and theoretical studies," Ph.D. thesis, Ecole Centrale de Lyon/Moscow State University, 2008.
[41]K. Kurganov and E. Tandmor, "New high-resolution central schemes for nonlinear conservation laws and convention-diffusion equations," J. Comput. Phys. **160**, 241–282 (2000).
[42]W.H. Press, S.A. Teukolsky, W.T. Vetterling, and B.P. Flannery, *Numerical Recipes in Fortran. The Art of Scientific Computing*, 2nd ed. (University Press, Cambridge, 1992), pp. 818–881.
[43]B.A. Davy and D.T. Blackstock, "Measurements of the refraction and diffraction of a short *N*-wave by a gas-filled soap bubble," J. Acoust. Soc. Am. **49**, 732–737 (1971).
[44]R. Marchiano, F. Coulouvrat, and R. Grenon, "Numerical simulation of shock wave focusing at fold caustics, with application to sonic boom," J. Acoust. Soc. Am. **114**, 1758–1771 (2003).
[45]K.J. Plotkin, "State of the art of sonic boom modeling," J. Acoust. Soc. Am. **111**, 530–536 (2002).
[46]B. Iooss, P. Blanc-Benon, and C. Lhuillier, "Statistical moments of travel times at second order in isotropic and anisotropic random media," Waves Random Media **10**, 381–394 (2000).
[47]T. Saito, "Velocity shift in two-dimensional anisotropic random media using the Rytov method," Geophys. J. Int. **166**, 293–308 (2006).